Computational Materials Science 67 (2013) 229–237

Contents lists available at SciVerse ScienceDirect

Computational Materials Science

journal homepage: www.elsevier.com/locate/commatsci

Design of 3D orthotropic materials with prescribed ratios for effective Young's moduli

X.Y. Yang [a], X. Huang [a], J.H. Rong [b], Y.M. Xie [a,*]

[a] Centre for Innovative Structures and Materials, School of Civil, Environmental and Chemical Engineering, RMIT University, GPO Box 2476, Melbourne 3001, Australia
[b] School of Automotive and Mechanical Engineering, Changsha University of Science and Technology, Changsha 410076, China

ARTICLE INFO

Article history:
Received 26 April 2012
Received in revised form 13 August 2012
Accepted 26 August 2012
Available online 9 October 2012

Keywords:
Topology optimization
Orthotropy
Homogenization
Bi-directional evolutionary structural method (BESO)
Lagrangian multipliers

ABSTRACT

An orthotropic material is characterized by nine independent moduli. The ratios between the Young's moduli in three directions are indicative of the level of orthotropy and the bulk modulus is indicative of the overall stiffness. In this paper we propose a method for designing the stiffest orthotropic material which has prescribed ratios for Young's moduli. The material is modeled as a microstructure in a periodic unit cell. By using the homogenization method, the elasticity tensors are calculated and its compliance matrix is derived. A Lagrangian function is constructed to combine the objective and multiple equality constraints. To enable a bi-section search algorithm, the upper and lower bounds on those multipliers are derived by using a strain energy approach. The overall optimization is based on the bi-directional evolutionary structural optimization (BESO) method. Examples of various orthotropy ratios are investigated. The topology presents a constant pattern of material re-distributed along the strongest axis while the overall stiffness is maintained.

1. Introduction

Composite and cellular materials are well known for their advanced properties and light weight. Composite materials are widely used in industries and their design and analysis techniques have been developed extensively, especially for laminate composites [1]. Natural cellular materials, such as cancellous bones and wood cells, have been investigated by experiments and modeling during the last several decades, most notably in the pioneer work by Cave and Hutt [2] and Gibson et al. [3]. The latest development includes a sophisticated 3D modeling of the multiple phases of the wood cell [4].

One interesting aspect of those advance materials is that they are anisotropic mechanically and thermally. Indeed, the superiority of the composite laminate to the common isotropic materials lies in its tailored anisotropy in reaction to the specific loading/environment conditions. The design conditions for natural materials are more complex and their mechanical properties are of significant interest from a bi-inspired design point of view. On the orthotropic elasticity of the wood cell [3], the three Young's moduli in longitudinal, radial and tangential directions are expressed as a function of the relative density with the longitudinal modulus the largest one. It is found that the ratio between the radial and tangential to the longitudinal moduli varies significantly from softwoods to hardwoods.

From an engineering design point of view, much work is devoted to optimizing the materials or structures so that they possess the desired or prescribed orthotropy. On a theoretical aspect, the bounds on the Young's moduli of the composite laminate are solved analytically [5]. For more specific applications, the density and orientation of the lamina layup are designed according to the optimal stress/stiffness criteria [6,7].

In this paper, we seek to design general 3D continuous materials which have the prescribed orthotropy. Material design, as a much investigated topic, has reached maturity over decades since the formulation of the homogenization method [8]. An extensive bibliography of relevant work can be found in the book by Bendsøe and Sigmund [9], covering various aspects of elasticity, thermal conductivity and acoustic properties.

Results on the elasticity have included the bulk and shear modulus and their combinations as well as Poisson's ratio [10,11]. Those results are mostly focused on isotropic materials or materials of square or cubic symmetrical. For orthotropic materials, design objectives/constraints of various forms have been investigated. In results on 2D materials [12], the four independent elasticity constants are constrained to their respective target value while the volume/weight is to be minimized. For 3D materials, to satisfy constraints on each of the nine independent constant is usually considered to be less achievable. In designing scaffold biomaterial [13], for example, the designed constants are reduced to

* Corresponding author. Tel.: +61 3 9925 3655; fax: +61 3 9639 0138.
E-mail address: mike.xie@rmit.edu.au (Y.M. Xie).

0927-0256/$ - see front matter © 2012 Elsevier B.V. All rights reserved.
http://dx.doi.org/10.1016/j.commatsci.2012.08.043

three Young's moduli and three shear moduli. Instead of satisfying each individual constant, a cost function is formulated which summarizes the difference between each individual to its target. Usually it needs *prior* knowledge to specify an appropriate target value. For example, to stimulate tissue generation the stiffness of the scaffolds tissue may be assumed to match that of the host bone.

In this paper we consider a more general orthotropic design problem in that there is no information on the absolute target value for each modulus. Instead, we specify the ratio between interested moduli, e.g., between the effective Young's moduli in three directions. They are more relaxed constraints than specifying an absolute target. The volume/weight can be included as an additional constraint. Without any further requirements, there exist multiple solutions which satisfy the constraints. Therefore, a combined objective function is defined in terms of the largest Young's modulus and the bulk modulus. This is detailed in Section 2.2.

The optimization method used here is based on the bi-directional evolutionary structural optimization (BESO). The basic idea of BESO is that by gradually removing and adding materials, the structure evolves towards an optimum. The extensive work on BESO has been included in various publications [14–17]. On the material design, BESO has solved the optimization of bulk/shear modulus and thermal conductivity [18,19].

A Lagrangian function is constructed to combine the objective function and the multiple constraints. The optimum is searched based on the sensitivity analysis and Lagrangian multipliers are solved at each iteration. Examples are presented to demonstrate the effectiveness of the proposed BESO procedure for solving problems of various orthotropic ratios.

2. Formulation of optimization problem

2.1. Elasticity properties by homogenization

The constitutive law of linear elasticity is given by

$$\boldsymbol{\sigma} = \mathbf{E}\boldsymbol{\varepsilon}, \tag{1a}$$

where for 3D $\boldsymbol{\sigma} = \{\sigma_{11}, \sigma_{22}, \sigma_{33}, \sigma_{12}, \sigma_{13}, \sigma_{23}\}$ and $\boldsymbol{\varepsilon} = \{\varepsilon_{11}, \varepsilon_{22}, \varepsilon_{33}, \gamma_{12}, \gamma_{13}, \gamma_{23}\}$. Making use of abbreviations of $11 \to 1$, $22 \to 2$,$33 \to 3$, $12 \to 4$, $13 \to 5$ and $23 \to 6$, $\boldsymbol{\sigma}$ and $\boldsymbol{\varepsilon}$ can be written as

$$\boldsymbol{\sigma} = \{\sigma_1, \sigma_2, \sigma_3, \sigma_4, \sigma_5, \sigma_6\} \tag{1b}$$

$$\boldsymbol{\varepsilon} = \{\varepsilon_1, \varepsilon_2, \varepsilon_3, \gamma_4, \gamma_5, \gamma_6\} \tag{1c}$$

For a heterogeneous material consists of different base materials, it is usually modeled as a microstructure of a periodical base cell (PBC) with *NE* finite elements. Using the homogenization theory [20], the elastic tensor is expressed as

$$E^H_{ij} = \sum_{e=1}^{NE} Q^e_{ij} = \sum_{e=1}^{NE} \left(\frac{1}{Y^e} \int_{Y^e} (\boldsymbol{\varepsilon}_i^{0^T} - \boldsymbol{\varepsilon}_i^T) \mathbf{E} (\boldsymbol{\varepsilon}_j^0 - \boldsymbol{\varepsilon}_j) dY_e \right)_e$$
$$(i,j = 1 \text{ to } 6 \text{ for 3D}), \tag{2}$$

where $\mathbf{E}$ is the elastic matrix of the base material, $\boldsymbol{\varepsilon}_i^0$ is the i-th unit test strain field and $\boldsymbol{\varepsilon}_i$ is the corresponding induced strain field. The implementation of the homogenization has become a standard procedure, as detailed in many literatures [e.g. 20]. For 3D material, it involves applying six cases of periodic boundary conditions and unit strain fields. Then the 6×6 $\mathbf{E}^H_{ij}$ make up the elasticity matrix $\mathbf{E}^H$.

The compliance matrix $\mathbf{C}^H$ is calculated as the inverse of the elasticity matrix $\mathbf{E}^H$, i.e.

$$\mathbf{C}^H = [C_{ij}] = \mathbf{E}^{H^{-1}}, \tag{3a}$$

where for orthotropic materials, $\mathbf{C}^H$ can be written in terms of nine elasticity constants, i.e.

$$\mathbf{C}^H = [C_{ij}] = \begin{bmatrix} \frac{1}{E_1} & \frac{-v_{21}}{E_2} & \frac{-v_{31}}{E_3} & 0 & 0 & 0 \\ \frac{-v_{12}}{E_1} & \frac{1}{E_2} & \frac{-v_{32}}{E_3} & 0 & 0 & 0 \\ \frac{-v_{13}}{E_1} & \frac{-v_{23}}{E_2} & \frac{1}{E_3} & 0 & 0 & 0 \\ 0 & 0 & 0 & \frac{1}{G_{12}} & 0 & 0 \\ 0 & 0 & 0 & 0 & \frac{1}{G_{13}} & 0 \\ 0 & 0 & 0 & 0 & 0 & \frac{1}{G_{23}} \end{bmatrix} \tag{3b}$$

The three effective Young's moduli, E_1, E_2 and E_3, as the focus of this paper, are defined as

$$E_i = \frac{1}{C_{ii}} \quad (i = 1 \text{ to } 3) \tag{4}$$

The bulk modulus K is defined as average of the 3×3 axial elastic tensors. It can be written in a strain energy form as

$$K = \boldsymbol{\varepsilon}^T \mathbf{E}^H \boldsymbol{\varepsilon}, \tag{5}$$

where $\boldsymbol{\varepsilon}$ is a third of the unit strain, i.e. $\boldsymbol{\varepsilon} = \frac{1}{3}\{1,1,1,0,0,0\}$. Omitting the shear components, the strain can be written as $\boldsymbol{\varepsilon} = \frac{1}{3}\{1,1,1\}$. The omission of shear components is applicable in the rest of the paper.

2.2. Objective function and multiple constraints

The design requirements on prescribed orthotropy can be stated as

$$E_1 = a_{13} E_3, \tag{6a}$$

$$E_2 = a_{23} E_3, \quad (0 < a_{13} \leqslant 1, 0 < a_{23} \leqslant 1) \tag{6b}$$

$$V_e x_e = V, \quad x_e = x_{\min} \text{ or } 1, \tag{6c}$$

where a_{13} and a_{13} are the orthotropy ratios, x_e is the design variable with $x_e = x_{\min}$ as void and $x_e = 1$ as solid, and V is the prescribed volume.

In formulating the optimization problem, the above three equations can be treated as constraints. Then the question is how to specify appropriate objective function(s). The most straight forward objective is to maximize the largest modulus E_3, i.e.

$$\text{Maximize} \quad E_3 \tag{6d}$$

It is found that there are multiple solutions to the above problem statement as Eqs. (6a)–(6d). Two candidate topologies are shown in Fig. 1 They have the same volume and their Young's modulus of the base material is E_0. With a near constant cross section, both topologies have their largest modulus E_3 approximating the maximum $E_3^{\max} = VE_0$. Their in-plane modulus E_1 and E_2 are close too, with $E_1 = E_2 = 0.5$ E_3 (i.e. $a_{13} = a_{23} = 0.5$). Therefore, the two topologies have both satisfied Eqs. (6a)–(6d). It is noted that topology 1 is close to a mechanism with very weak link around joints. It has a much lower bulk modulus, i.e. 1.10 compared to 2.08 for topology 2. As in most cases it is desirable that the structure has a high overall stiffness, the bulk modulus is to be included as an objective in addition to the largest modulus E_3.

A further example is on maximizing the bulk modulus only without considering the largest modulus E_3. Two candidate topologies are shown in Fig. 2 with their elasticity matrice. The bulk moduli, effective moduli and Poisson's ratios are compared in Table 1. It is seen that values of the bulk modulus, as the single objective, are very close. Topology 2 is similar to the I-WP surface [21] which has its three orthogonal panels aligned with three

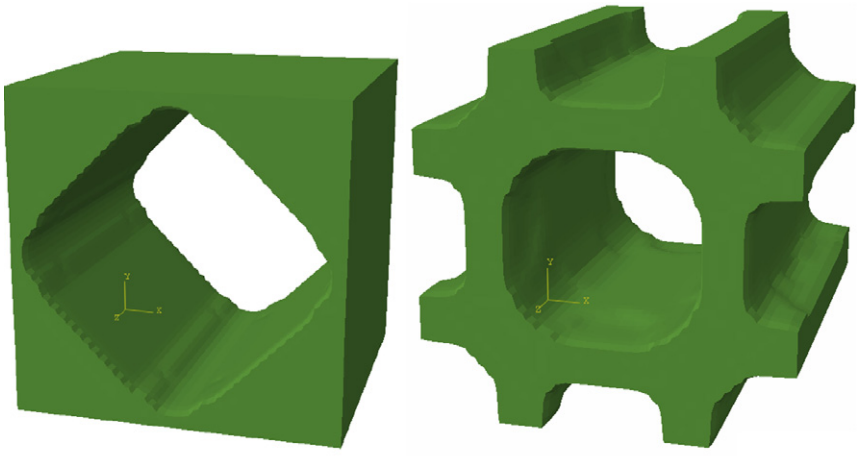

(a) Topology 1 (b) Topology 2

Fig. 1. Comparison of bulk modulus K of two topologies for $a_{13} = a_{23} = 0.5$.

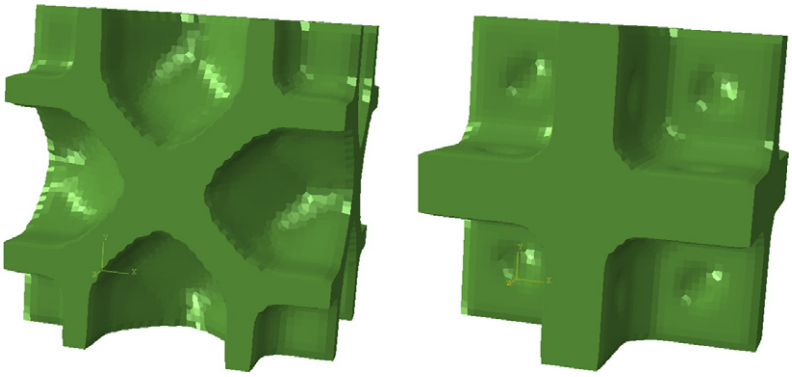

(a) Topology 1 (b) Topology 2

$$E^H = \begin{bmatrix} 0.386 & 0.144 & 0.144 & 0 & 0 & 0 \\ 0.144 & 0.386 & 0.144 & 0 & 0 & 0 \\ 0.144 & 0.144 & 0.386 & 0 & 0 & 0 \\ 0 & 0 & 0 & 0.114 & 0 & 0 \\ 0 & 0 & 0 & 0 & 0.114 & 0 \\ 0 & 0 & 0 & 0 & 0 & 0.114 \end{bmatrix} \quad E^H = \begin{bmatrix} 0.440 & 0.115 & 0.115 & 0 & 0 & 0 \\ 0.115 & 0.440 & 0.115 & 0 & 0 & 0 \\ 0.115 & 0.115 & 0.440 & 0 & 0 & 0 \\ 0 & 0 & 0 & 0.098 & 0 & 0 \\ 0 & 0 & 0 & 0 & 0.098 & 0 \\ 0 & 0 & 0 & 0 & 0 & 0.098 \end{bmatrix}$$

Fig. 2. Comparison of effective Young's modules for $a_{13} = a_{23} = 1.0$.

Table 1
Comparison of two topologies with maximum bulk modulus K.

	Topology 1	Topology 2
K	0.225	0.224
$E_1(=E_2=E_3)$	0.307	0.392
$\nu_{12}(=\nu_{13}=\nu_{23})$	0.272	0.208

principle axes. This gives rise to significantly higher moduli and lower Poisson's ratios.

From the argument above, it is necessary to include both the bulk modulus and the largest modulus in the objective function. Therefore, the optimization problem is specified as

$$\text{Minimize} \quad f_{obj} = \frac{1}{E_3} + \frac{1}{K} \tag{7a}$$

$$\text{Subject to} \quad f_{c13} = \frac{1}{E_1} - \frac{1}{a_{13}}\frac{1}{E_3} = 0, \tag{7b}$$

$$f_{c23} = \frac{1}{E_2} - \frac{1}{a_{23}}\frac{1}{E_3} = 0, \quad (0 < a_{13} \leqslant 1, 0 < a_{23} \leqslant 1), \tag{7c}$$

$$V_e x_e = V, \quad x_e = x_{\min} \text{ or } 1, \tag{7d}$$

Using Eq. (4), the constraints are re-written as

$$f_{c13} = C_{11} - \frac{1}{a_{13}} C_{33} = 0, \tag{8a}$$

$$f_{c23} = C_{22} - \frac{1}{a_{23}} C_{33} = 0, \tag{8b}$$

$$f_{c12} = C_{11} - \frac{1}{a_{12}} C_{22} = 0, \quad \left(a_{12} = \frac{a_{13}}{a_{23}}\right) \tag{8c}$$

where Eq. (8c) is derived from Eqs. (8a and b). It becomes redundant only when the first two constraints are *both* satisfied.

The Lagrangian function combing the objective function and constraints is defined as

$$f_L = C_{33} + \frac{1}{K} + \lambda_{13}\left(C_{11} - \frac{1}{a_{13}}C_{33}\right) + \lambda_{23}\left(C_{22} - \frac{1}{a_{23}}C_{33}\right) + \lambda_{12}\left(C_{11} - \frac{1}{a_{12}}C_{22}\right), \tag{9}$$

where $\lambda_{13}, \lambda_{23}$ and λ_{12} are the Lagrangian multipliers.

2.3. Bounds on Lagrangian multipliers

In determining the value for the Lagrangian multiplier, usually it is searched from an initial value and then adjusted within a given range. In this paper, the range or the bounds on the three Lagrangian multipliers are calculated based on the concept of strain energy density.

Suppose a unit cell of a compliance matrix $\mathbf{C}^H$ is subject to an arbitrary axial stress vector $\boldsymbol{\sigma} = \{\sigma_2, \sigma_2, \sigma_3\}$. Omitting the coefficient 1/2, the strain energy density is

$$\Pi = \boldsymbol{\sigma}^T \mathbf{C}^H \boldsymbol{\sigma} = \sum_{i,j=1}^{3} \sigma_i \sigma_j C_{ij} \tag{10}$$

The bulk modulus in Eq. (5) can be written in a similar form as

$$K = \boldsymbol{\varepsilon}^T \mathbf{E}^H \boldsymbol{\varepsilon} = (\mathbf{E}^H \boldsymbol{\varepsilon})^T \mathbf{C}^H (\mathbf{E}^H \boldsymbol{\varepsilon}) = \boldsymbol{\sigma}^{K^T} \mathbf{C}^H \boldsymbol{\sigma}^K = \sum_{i,j=1}^{3} \sigma_i^K \sigma_j^K C_{ij}\,, \tag{11a}$$

where $\boldsymbol{\sigma}^K$ is the stress due to a third of the unit strain, i.e.

$$\boldsymbol{\sigma}^K = \mathbf{E}^H \boldsymbol{\varepsilon} = \frac{1}{3}\begin{bmatrix} E_{11}^H & E_{12}^H & E_{13}^H \\ E_{21}^H & E_{22}^H & E_{23}^H \\ E_{31}^H & E_{32}^H & E_{33}^H \end{bmatrix}\begin{Bmatrix} 1 \\ 1 \\ 1 \end{Bmatrix} = \frac{1}{3}\begin{Bmatrix} E_{11}^H + E_{12}^H + E_{13}^H \\ E_{21}^H + E_{22}^H + E_{23}^H \\ E_{31}^H + E_{32}^H + E_{33}^H \end{Bmatrix} = \begin{Bmatrix} \sigma_1^K \\ \sigma_2^K \\ \sigma_3^K \end{Bmatrix} \tag{11b}$$

Using Eqs. (11a and b), the Lagrangian function in Eq. (9) can be written as

$$K^2 f_L = \boldsymbol{\sigma}^K \mathbf{C}_\lambda \boldsymbol{\sigma}^K, \tag{12a}$$

where

$$\mathbf{C}_\lambda = \begin{bmatrix} C_{11}\left(1 + \left(\frac{K}{\sigma_1^K}\right)^2 (\lambda_{13} + \lambda_{12})\right) & C_{12} & C_{13} \\ C_{21} & C_{22}\left(1 + \left(\frac{K}{\sigma_2^K}\right)^2 \left(\lambda_{23} - \frac{\lambda_{12}}{a_{12}}\right)\right) & C_{23} \\ C_{31} & C_{32} & C_{33}\left(1 + \left(\frac{K}{\sigma_3^K}\right)^2 \left(1 - \frac{\lambda_{13}}{a_{13}} - \frac{\lambda_{23}}{a_{23}}\right)\right) \end{bmatrix} \tag{12b}$$

In this form, $\mathbf{C}_\lambda$ can be regarded as the compliance matrix of a certain fictitious material. One of the requirements of material stability is that its three diagonal terms are positive, i.e.

$$\left(\frac{\sigma_1^K}{K}\right)^2 + \lambda_{13} + \lambda_{12} \geqslant 0 \tag{13a}$$

$$\left(\frac{\sigma_2^K}{K}\right)^2 + \lambda_{23} - \frac{\lambda_{12}}{a_{12}} \geqslant 0 \tag{13b}$$

$$\left(\left(\frac{\sigma_3^K}{K}\right)^2 + 1\right) - \left(\frac{\lambda_{13}}{a_{13}} + \frac{\lambda_{23}}{a_{23}}\right) \geqslant 0 \tag{13c}$$

The above three inequalities implicitly set the upper and lower bounds on the Lagrangian multipliers. They are not sufficient to solve the total 3×2 bounds, and certain assumptions are to be considered. The principle is that the two primary constraints are evaluated first then followed by the secondary constraint. This two level approach is detailed as follows.

2.3.1. Level 1 – Determine the bounds on the two primary multipliers

Here we assume that the secondary multiplier $\lambda_{12} = 0$, then Inequalities (13a and b) become

$$\lambda_{13} \geqslant -\left(\frac{\sigma_1^K}{K}\right)^2 \tag{14a}$$

$$\lambda_{23} \geqslant -\left(\frac{\sigma_2^K}{K}\right)^2, \tag{14b}$$

which set the lower bounds of λ_{13} and λ_{23}.

Approximation is made when solving the upper bounds of λ_{13} and λ_{23} from Inequality (13c). The inequality is sufficiently satisfied when the following two inequalities are satisfied, i.e.

$$\frac{a_{13}}{a_{13} + a_{23}}\left(\left(\frac{\sigma_3^K}{K}\right)^2 + 1\right) - \frac{1}{a_{13}}\lambda_{13} \geqslant 0 \tag{15a}$$

$$\frac{a_{23}}{a_{13} + a_{23}}\left(\left(\frac{\sigma_3^K}{K}\right)^2 + 1\right) - \frac{1}{a_{23}}\lambda_{23} \geqslant 0 \tag{15b}$$

Solving the above leads to

$$\lambda_{13} \leqslant \frac{a_{13}^2}{a_{13} + a_{23}}\left(\left(\frac{\sigma_3^K}{K}\right)^2 + 1\right) \tag{15c}$$

$$\lambda_{23} \leqslant \frac{a_{23}^2}{a_{13} + a_{23}}\left(\left(\frac{\sigma_3^K}{K}\right)^2 + 1\right) \tag{15d}$$

As Inequalities (15c and d) are sufficient conditions of Inequality (13c), they represents a more restrictive upper bound on λ_{13} and λ_{23}. Then the question is whether such a restriction will affect the overall search path, which is discussed as below.

When applying the homogenization to calculate the 3D material properties, the periodic base cell is usually modeled as a cubic design domain. In the initial design, the domain has a small sub-domain of cube or sphere at the centre which is voids or soft materials. This initial design is cubic symmetrical, i.e. $C_{11} = C_{22} = C_{33}$, and therefore constraints as Eqs. (8a and 8b) are non-positive.

Materials are to be re-distributed among the domain as the volume is gradually reduced to the target V. As the result of the volume reduction, the three Young's moduli will decrease from their initial values, or the corresponding compliance C_{11}, C_{22} and C_{33} will increase. To maintain C_{33} to be the smallest among the three (i.e. the strongest modulus), C_{11} and C_{22} will increase more significantly than C_{33}. The change of C_{11}, C_{22} and C_{33} is such that the constraints are better satisfied as the optimization proceeds, i.e. from the initial non-positive value to gradually approaching 0.

When the constraint is negative, the Lagrangian multipliers are searched only in the negative set, i.e. $\lambda_{13} \in \left[-\left(\frac{\sigma_1^K}{K}\right)^2, 0\right]$ and $\lambda_{23} \in \left[-\left(\frac{\sigma_2^K}{K}\right)^2, 0\right]$ according to Inequalities (14a and b). Therefore the upper bounds as Inequalities (15c and d) are inactive. When the constraints approach 0, they are very close to convergence and their absolute values are very small. From this point, it only takes fine-tuning of λ_{13} and λ_{23} to reach the convergence. Their upper bound may become active during fine-tuning. As the absolute values of λ_{13} and λ_{23} are very small too, the effect of restriction on the upper bound will be insignificant.

Combing Inequality (14a and b) and (15c and d), the upper and lower bounds can be written as

$$-\left(\frac{\sigma_i^K}{K}\right)^2 \leqslant \lambda_{i3} \leqslant \frac{a_{i3}^2}{a_{i3} + a_{(3-i)3}}\left(\left(\frac{\sigma_3^K}{K}\right)^2 + 1\right), \quad i = 1, 2, \tag{16}$$

2.3.2. Level 2 – Determine the bounds on the secondary multiplier

Based on the bounds as defined above, the values of λ_{13} and λ_{23} are determined (detailed in Section 4.3.2). Those values are then

substituted to inequalities (13a and b) and the bounds on λ_{12} are obtained, i.e.

$$-\left(\left(\frac{\sigma_1^K}{K}\right)^2+\lambda_{13}\right)\leqslant\lambda_{12}\leqslant a_{12}\left(\left(\frac{\sigma_2^K}{K}\right)^2+\lambda_{23}\right) \tag{17}$$

It is noted when λ_{13} and λ_{23} are very close to their respective lower bounds $-\left(\frac{\sigma_1^K}{K}\right)^2$ and $-\left(\frac{\sigma_2^K}{K}\right)^2$, the upper and lower bounds on λ_{12} are both close to 0. This is the case at the early stage of iteration. Throughout iterations the absolute value of λ_{12} remains small. It is usually lower than λ_{13} and λ_{23} by 2–3 orders.

3. Sensitivity analysis

3.1. Sensitivity analysis of elasticity and compliance constants

The sensitivity of the Lagrangian function is

$$\begin{aligned}\frac{\partial f_L}{\partial x_e}=&-\frac{1}{K^2}\frac{\partial K}{\partial x_e}+\frac{\partial C_{33}}{\partial x_e}+\lambda_{13}\left(\frac{\partial C_{11}}{\partial x_e}-\frac{1}{a_{13}}\frac{\partial C_{33}}{\partial x_e}\right)\\&+\lambda_{23}\left(\frac{\partial C_{22}}{\partial x_e}-\frac{1}{a_{23}}\frac{\partial C_{33}}{\partial x_e}\right)+\lambda_{12}\left(\frac{\partial C_{11}}{\partial x_e}-\frac{1}{a_{12}}\frac{\partial C_{22}}{\partial x_e}\right),\end{aligned} \tag{18}$$

which calls for the sensitivity analysis of the elasticity and compliance constants.

The sensitivity of the elasticity can be conducted by using the adjoint method [9]. The sensitivity of E_{ij}^H is

$$\frac{\partial E_{ij}^H}{\partial x_e}=\frac{1}{Y^e}\int_{Y^e}\left(\boldsymbol{\varepsilon}_i^{0^T}-\boldsymbol{\varepsilon}_i^T\right)\frac{\partial\mathbf{E}}{\partial x_e}(\boldsymbol{\varepsilon}_j^0-\boldsymbol{\varepsilon}_j)dY_e. \tag{19}$$

The term $\frac{\partial\mathbf{E}}{\partial x_e}$ depends on the scheme used to interpolate the Young's modulus E. Here the interpolation function is based on the widely used SIMP method [22], i.e.

$$E(x_e)=x_e^pE_0, \tag{20}$$

where E_0 are the Young's modulus of the base materials and p is the power of penalty. It represents voids when $x_e=x_{\min}$ (e.g. 10^{-5}).

The sensitivity analysis of the bulk modulus $\frac{\partial K}{\partial x_e}$ is calculated by combining Eqs. (5) and (19).

The sensitivity of the mean compliance matrix $\mathbf{C}^H$ is calculated by using the chain rule. The sensitivity of the 3×3 axial components is

$$\frac{\partial C_{ij}}{\partial x_e}=\sum_{k,l=1}^{3}\frac{\partial C_{ij}}{\partial E_{kl}^H}\frac{\partial E_{kl}^H}{\partial x_e}\quad(i,j=1\text{ to }3) \tag{21}$$

The inverse of a 3×3 matrix can be solved analytically and thus C_{ij} and $\frac{\partial C_{ij}}{\partial E_{kl}}$ are explicit functions of E_{kl}. Therefore, $\frac{\partial C_{ij}}{\partial x_e}$ can be calculated analytically by following series of matrix operations.

3.2. Sensitivity number

The above sensitivity analysis is the basis of the sensitivity number which is the searching criteria used in BESO. The sensitivity number from Eq. (18) is defined as

$$\alpha_e=-\frac{\partial f_L}{\partial x_e} \tag{22}$$

The sensitivity number α_e is then filtered through a spherical range of radius $r_{\min}$ to obtain a weighted 'average', i.e.

$$\tilde{\alpha}_e=f(\alpha_e) \tag{23}$$

Taken the centre of an brick element e as reference, neighbor elements within the radius $r_{\min}$ are taken into account to contribute to the sensitivity of element e. The contribution depends on the sensitivity of the each individual neighbor element and its distance to element e. Details of the filter methodology are presented in Ref. [17].

The sensitivity of the mean compliance $\mathbf{C}^H$ is filtered in the same way, i.e.

$$\frac{\partial\widetilde{C}_{ij}}{\partial x_e}=f\left(\frac{\partial C_{ij}}{\partial x_e}\right) \tag{24}$$

Assuming there are totally m elements modified, the increment of $\mathbf{C}^H$ is then

$$\Delta C_{ij}\approx\sum_{e=1}^{m}\frac{\partial\widetilde{C}_{ij}}{\partial x_e}\Delta x_e \tag{25}$$

The predicted mean compliance after the modification is

$$C'_{ij}\approx C_{ij}+\Delta C_{ij}^H \tag{26}$$

4. Optimization procedures

Like most methods based on the sensitivity analysis, BESO proceeds the search iteratively until certain criteria are satisfied. Parameters and criteria are detailed in this section.

4.1. Parameters

There are two parameters which control the step length of iteration, that is, the evolutionary ratio ER and the maximum ratio R max . Assume that there are totally NE elements in the design domain and the volume constraint is V. The volume of the current and the next iterations is V^k and V^{k+1}, respectively. V^{k+1} is predicted as $V^{k+1}=V^k(1-ER)$ and it is corresponding to $NE\times V^{k+1}$ number of solid elements. The threshold for element modification is set as

$$NE_{thre}=NE\times V^{k+1}=NE\times V^k(1-ER) \tag{27}$$

The modification according to the threshold is conducted as follows. Sorting the sensitivity numbers of the NE elements in a descend order, void elements above the threshold NE_{thre} are added and solid elements below the threshold are removed. As a result, the total numbers of elements removed and added are NR and NA, respectively. To ensure that only a small amount of elements are modified at each step, the ratio to the total element is less than a prescribed maximum ratio, i.e.

$$\frac{NR+NA}{NE}\leqslant R_{\max} \tag{28}$$

If the ratio is exceeded, elements are further down selected from the sets of NR and NA elements, while maintaining the ratio between NR and NA, i.e.

$$NR'=R_{\max}\times NE\times\frac{NR}{NR+NA} \tag{29a}$$

$$NA'=R_{\max}\times NE\times\frac{NA}{NR+NA} \tag{29b}$$

4.2. Convergence criteria

From the problem statement as Eqs. (6a)–(6d), (7a)–(7c), the relative difference of the two orthotropy ratios is defined as

$$\Delta a=\sqrt{\left(\left(\frac{C_{33}}{C_{11}}-a_{13}\right)/a_{13}\right)^2+\left(\left(\frac{C_{33}}{C_{22}}-a_{23}\right)/a_{23}\right)^2} \tag{30}$$

The evolution is considered to be convergent when all the following criteria are satisfied:

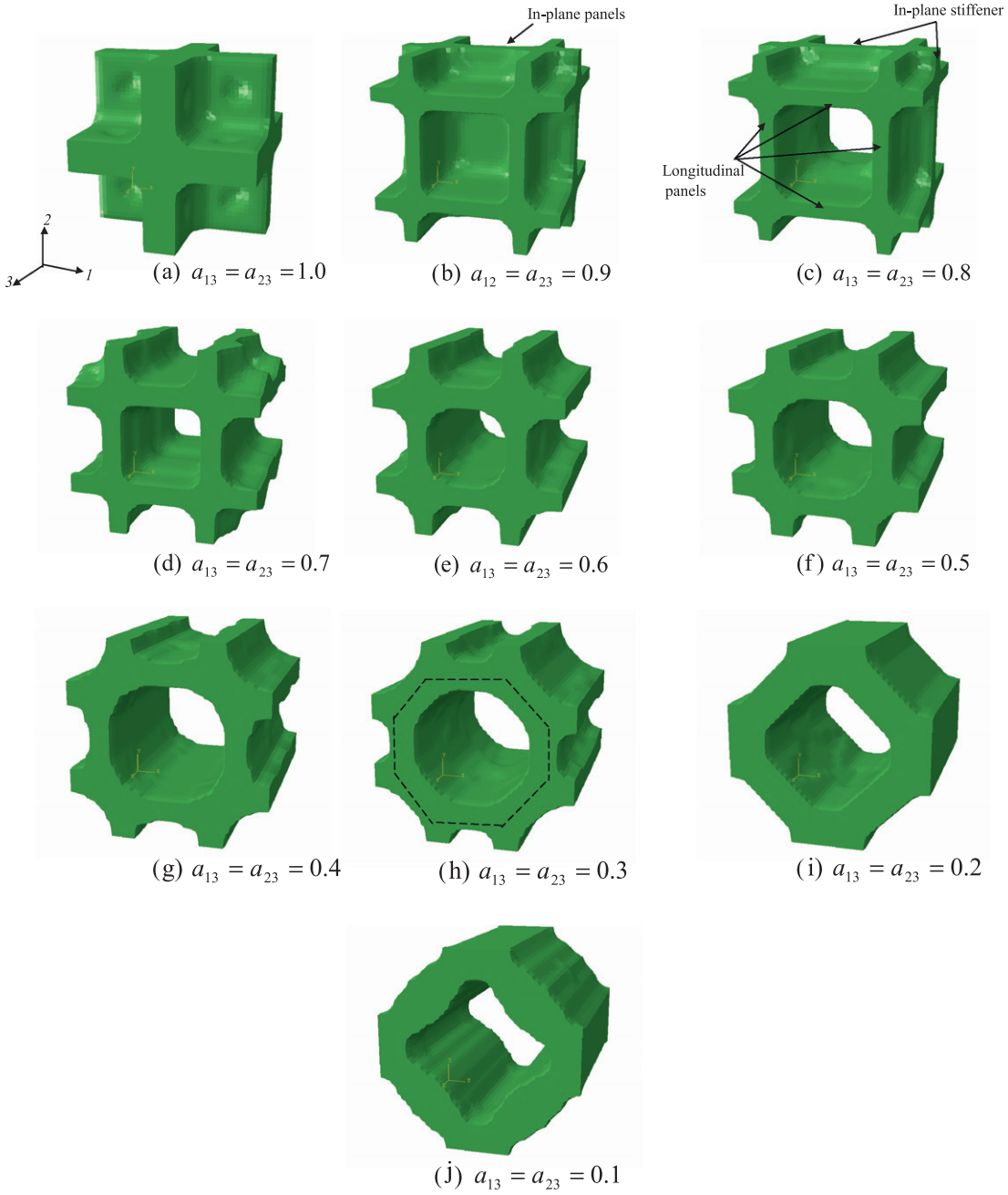

Fig. 3. Topologies for various cases of $a_{13} = a_{23}$.

(1) The volume constraint V is satisfied.
(2) The change in the bulk modulus ΔK is stabilized, i.e. the relative difference between the current iteration and the average of the last 10 iterations is small, e.g. $\Delta K \leqslant \tau_{obj}$, where τ_{obj} is usually set as 1%.
(3) The relative orthotropy difference Δa satisfies $\Delta a \leqslant \tau_{con}$, where τ_{con} is usually set as 1%.

4.3. Procedures

4.3.1. The overall procedure

The BESO procedure is as follows:

1. Discretize the periodic base cell with finite elements and define the initial design.
2. Apply the periodic boundary conditions and corresponding unit strain fields.
3. For each boundary and strain case, conduct finite element analysis to obtain the induced strain field $\boldsymbol{\varepsilon}$.
4. Calculate the elasticity matrix $\mathbf{E}^H$ and the compliances matrix $\mathbf{C}^H$.
5. Determine the three Lagrangian multipliers $\lambda_{13}, \lambda_{23}$ and λ_{12}. This calls for an inner loop to search the convergence of the multipliers. Detailed procedures are presented in Section 4.3.2.
6. Calculate the sensitivity number $\tilde{\alpha}_e$ using Eqs. (18)–(23).
7. Update the topology according to $\tilde{\alpha}_e$. As detailed in Section 4.1, the elements modified are decided by the threshold NE_{thre}.
8. Steps 2–7 are repeated until the convergence criteria as defined in Section 4.2 are satisfied.

4.3.2. Determining Lagrangian multipliers

4.3.2.1. Procedure. At each iteration of the overall optimization, the three Lagrangian multipliers are to be solved. The two primary multipliers $\lambda_{i3} (i = 1, 2)$ are solved first followed by the secondary

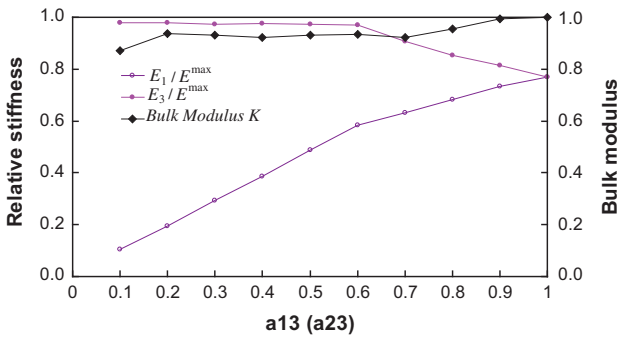

Fig. 4. Bulk modulus K and effective Young's modulus $E_1(=E_2)$ and E_3 for various cases of $a_{13} = a_{23}$.

multiplier λ_{12}. The procedure is as follows. Again it is assumed that the design domain has *NE* elements and the volume constraint is *V*.

1. Calculate the upper and lower bounds of λ_{i3} using Eq. (16), which are denoted as λ_{i3}^{upper} and λ_{i3}^{lower}. Then λ_{i3} are solved as follows.
2. For the current iteration m, assign values to the three Lagrangian multipliers. At iteration 1 the initial values are $\lambda_{i3}^0 = 0$ and $\lambda_{12}^0 = 0$.
3. Calculate the sensitivity number $\tilde{\alpha}_e$ using Eqs. (18)–(23).
4. Obtain an assumed topology which has the volume equal to the constraint *V*. This is similar to step 7 in Section 4.3.1. Now the threshold is $NE_{thre} = NE \times V$. That is, sorting all elements according to their sensitivity in a descend order, solid elements above the threshold are assumed to be removed and void elements below added.
5. For the assumed new topology, estimate the compliance matrix C_{jj} ($j = 1, 3$) using Eqs. (24)–(26). Calculate the two primary constraints f_{ci3} using Eqs. (8a and b).
6. Check the convergence of λ_{i3} using the following criteria:
   (a) Both constraints are satisfied, i.e. $f_{ci3} = 0$ or $|f_{ci3}| \leqslant 1.0 \times 10^{-5}$.
   (b) If 9a) is not satisfied, the change in f_{ci3} between the current and the last iterations is small, i.e. $|f_{ci3}^m - f_{ci3}^{m-1}| < 1.0 \times 10^{-5}$.
7. If either of λ_{i3} has not converged, update λ_{i3} according to the bi-section rule:
   (a) If $f_{ci3} > 0$, then $\lambda_{i3}^{m+1} = \frac{1}{2}(\lambda_{i3}^m + \lambda_{i3}^{upper})$, and the lower bound is reset as $\lambda_{i3}^{lower} = \lambda_{i3}^m$.
   (b) If $f_{ci3} < 0$, then $\lambda_{i3}^{m+1} = \frac{1}{2}(\lambda_{i3}^m + \lambda_{i3}^{lower})$, and the upper bound is reset as $\lambda_{i3}^{upper} = \lambda_{i3}^m$.
8. Proceed to iteration $m + 1$, repeat steps 3–7 until convergence.
9. After both λ_{i3} have converged, substitute them to Eq. (17) to calculate the bounds on λ_{12}. Then λ_{12} is solved as follows.
10. For the current step n, assign value to λ_{12}. At iteration 1 the initial values is $\lambda_{12}^0 = 0$.
11. Calculate the sensitivity number $\tilde{\alpha}_e$ using Eqs. (18)–(23).
12. Obtain an assumed topology which has the volume equal to the constraint *V*, same as Step 4.
13. Estimate the compliance matrix C_{jj} ($j = 1, 3$) using Eqs. (24)–(26). Calculate the secondary constraint f_{c12} using Eq. (8c).
14. Check the convergence of λ_{12} using the following criteria:
   (a) The constraints is satisfied, i.e. $f_{c12} = 0$ or $|f_{c12}| \leqslant 1.0 \times 10^{-5}$.
   (b) If (a) is not satisfied, the change in f_{c12} between the current and last iterations is small, i.e. $|f_{c12}^n - f_{c12}^{n-1}| < 1.0 \times 10^{-5}$.
15. If λ_{12} has not converged, update it as follows:
   (a) If $f_{c12} > 0$, then $\lambda_{12}^{n+1} = \frac{1}{2}(\lambda_{12}^n + \lambda_{12}^{upper})$, and the $\lambda_{12}^{lower} = \lambda_{12}^n$.
   (b) If $f_{c12} < 0$, then $\lambda_{12}^{n+1} = \frac{1}{2}(\lambda_{12}^n + \lambda_{12}^{lower})$, and the upper bound is reset as $\lambda_{i3}^{upper} = \lambda_{12}^n$.
16. Proceed to iteration $n + 1$, repeat steps 11–15 until convergence.

4.3.2.2. Correction of the orthotropy ratios. At the early stage of the optimization, the volume is far from its target constraint *V*. At Step 5 which evaluates f_{ci3} at the target volume, it can be found that $f_{ci3} = C_{ii} - \frac{1}{a_{i3}} C_{33} \ll 0$. This means that a_{i3} is too low to achieve from the *current* topology. Assume that a more realistic constraint is satisfied, i.e.

$$f'_{ci3} = C_{ii} - \frac{1}{a'_{i3}} C_{33} = 0 \tag{31}$$

Then a new ratio is found to be

$$a'_{i3} = \frac{C_{33}}{C_{ii}} \tag{32}$$

This ratio is used as a correction to the actual ratio, i.e.

$$\bar{a}_{i3} = \frac{1}{2}(a_{i3} + a'_{i3}) \tag{33}$$

The corrected ratio $\bar{a}_{i3}$ is then used for the subsequent sensitivity analysis, as Step 6 of Section 4.3.1.

5. Examples

The periodic base cell is modeled as a cubic design domain which is divided by a $40 \times 40 \times 40$ mesh. Eight-node brick elements are used and they are of unit size. The material properties are Young's modulus $E_0 = 1.0$ and the Poisson's ratio of $\nu = 0.3$. $x_{min} = 10^{-5}$ and $p = 3$ are used in the interpolation scheme.

The initial design consists of a sphere of soft material in the cubic centre and the sphere radius is 4.0. Due to symmetry only a quarter mesh is used, i.e., $20 \times 20 \times 20$. The initial topology is orthotropic and also cubic symmetrical, i.e. $E_{11} = E_{22} = E_{33}$ and $C_{11} = C_{22} = C_{33}$.

The parameters used are volume constraint $V = 0.5$, evolution rate $ER = 1\%$, maximum Ratio $R_{max} = 2.5\%$ and filter radius $r = 4.6$ which is approximately 1/10 of the side length. The convergence tolerances are $\tau_{obj} = 1\%$ and $\tau_{con} = 1\%$. In presenting the results, the FE model is smoothened based on the curve and surface fitting.

Cases of both equal and unequal orthotropic ratios are studied as follows.

(1) Equal orthotropic ratios, i.e. $a_{13} = a_{23}$.

There are totally 10 cases, i.e. $a_{13} = a_{23} = 1.0$–0.1 with a decrement of 0.1. Results of topologies for those cases are shown in Fig. 3. Starting with $a_{13} = a_{23} = 1.0$, the topology is similar to the I-WP surface as discussed in Section 2.2. Materials are mainly distributed on three orthogonal panels which contribute to high values of three moduli E_1, E_2 and E_3.

When the panels in-plane of axes 1 and 2 becomes thinner, the two in-plane moduli E_1 and E_2 are reduced. This is shown in the topology for $a_{13} = a_{23} = 0.9$ (Fig. 3b). From $a_{13} = a_{23} = 0.9$ down to 0.8, the major change is the forming of cavity which reduces the in-plane panel to four continuous stiffeners. With $a_{13} = a_{23} = 0.7$, the stiffeners are discontinued and remain only on the four corners. Materials from those stiffeners are re-distributed to the four longitudinal panels which have seen increase in their thickness.

With $a_{13} = a_{23}$ further down to 0.6, the in-plane stiffeners are all removed. The four longitudinal panels form a cylinder-like topology. The longitudinal modulus E_3 is very close to the maximum

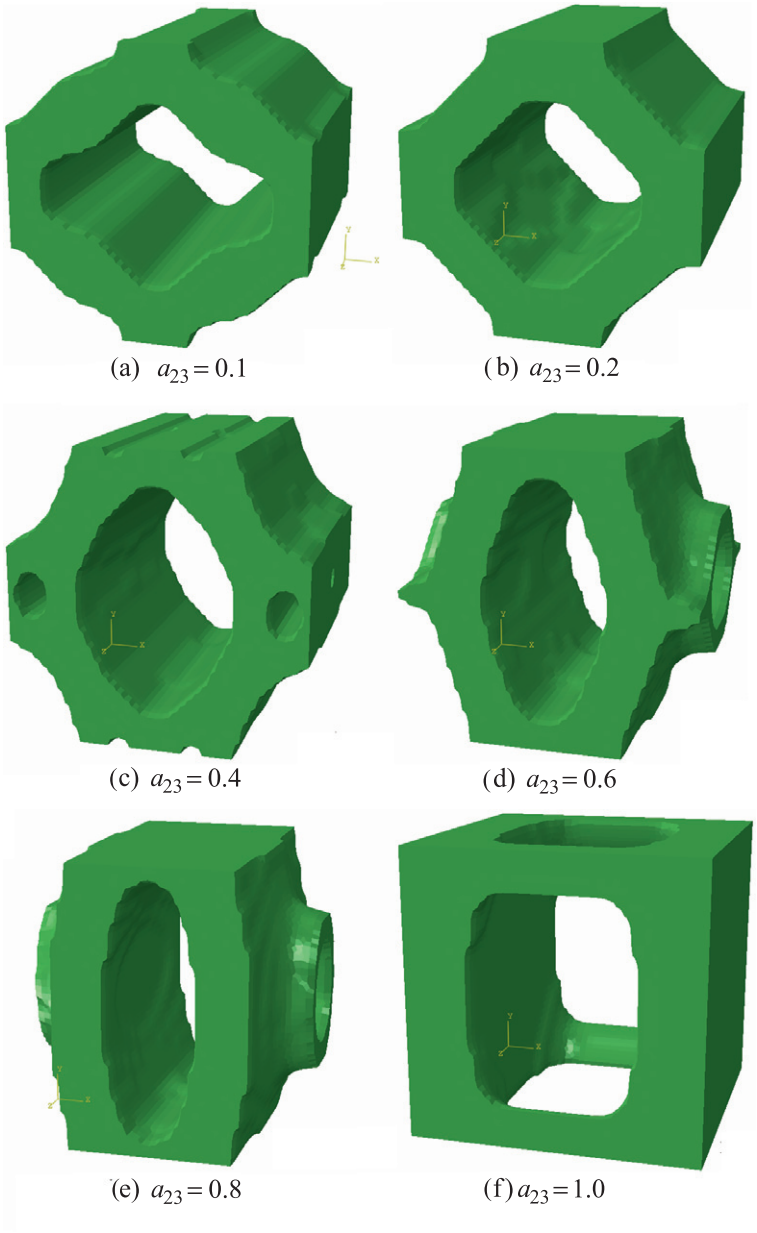

Fig. 5. Topologies for cases of $a_{12}=0.2$ with varying a_{23}.

value of 0.5. From this point, the topology appears to remain a cylinder and major changes are made in the in-plane or cross section. In the cross section at $a_{13}=a_{23}=0.6$, it features horizontal and vertical members which are almost orthogonal (in line with axes 1 and 2). This gives rise a relative high in plane moduli E_1 and E_2.

For $a_{13}=a_{23}=0.5$, the members are not as orthogonal with the forming of fillet like corners. The fillets become more distinct with $a_{13}=a_{23}$ further reduced. At $a_{13}=a_{23}=0.3$, the cross section is similar to an octagonal shape. The four diagonal sides of the octagon become more inclined and it is reduced to a diamond shape at $a_{13}=a_{23}=0.2$. It has very low in-plane moduli as the 45° member is the least effective in sustain the axial stress. With $a_{13}=a_{23}$ lowered further, the angle remains 45° and the profile of the member itself is changed. It appears that the material accumulated in the middle of the 45° member has very small contribution to the in-plane moduli.

The change of modulus of the above cases is presented in Fig. 4. From $a_{13}=a_{23}=1.0$. The longitudinal modulus E_3 increases and approaches its maximum E_3^{max} around $a_{13}=a_{23}=0.6$. It only changes slightly from 0.6 to 0.1. The in-pane modulus $E_1(=E_2)$ is reduced. With E_3 approaching maximum E_1 reduces more significantly from $a_{13}=a_{23}=0.6$ to 0.1. The overall stiffness has retained as the bulk modulus K is relatively high in all cases (above 80%).

(1) Unequal orthotropic ratios, i.e. $a_{13}=a_{23}$.

There are totally 6 cases, with $a_{13}=0.2$ and $a_{23}=0.1$, 0.2, 0.4, 0.6, 0.8 and 1.0, respectively. The topologies are as shown in Fig. 5. For $a_{13}=a_{23}=0.2$ as studied in the previous cases (Fig. 3i), the topology is similar to a cylinder with a diagonal square cross section. For $a_{23}<a_{13}=0.1$, the square are shortened in axis 2 and becomes a shallow diamond like shape. For $a_{23}>a_{13}$, the cavities are elongated in axis 2. For $a_{23}=1.0$, same cavity are formed at four planes which gives rise to $E_2=E_3$. The iteration history for the case $a_{13}=0.2$ and $a_{23}=0.4$ is shown in Fig. 6. E_1 and E_2 reduces together until E_2 reaches its target (0.4). Then E_1 is further reduced. At convergence they both approach their respective targets.

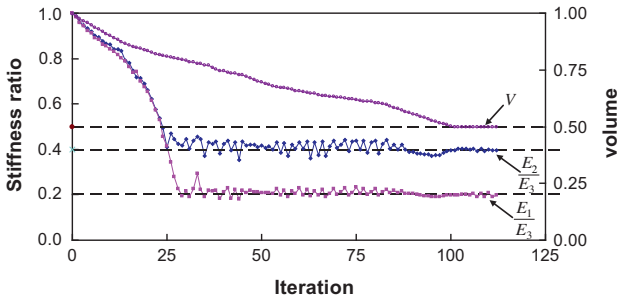

Fig. 6. Iteration history of effective Young's modules E_1 and E_2 for case of $a_{12} = 0.2$ and $a_{23} = 0.4$.

6. Conclusion

In the present study we have developed a technique to design the strongest orthotropic material which has the prescribed level of orthotropy. While the orthotropy can be very distinctive, i.e. low values of a_{13} and

a_{23}, the bulk modulus does not drop significantly from the reference topology of a cubic symmetrical design. From a cubic symmetrical initial design, the case of $a_{13} = a_{23} = 1$ has three equal Young's moduli. With lowered values of a_{13} and a_{23}, the largest moduli E_3 is increased and the smaller moduli is decreased. The obtained topologies exhibit a constant pattern of material being redistributed from the weak axis to the strong one. It finally becomes a cylinder-like structure which has the largest modulus E_3 approximating its maximum.

The implementation of the optimization procedure consists of an outer loop which updates the topology based on the sensitivity, and an inner loop which solved the three Lagrangian multipliers by using the bi-section method. The effectiveness of the proposed BESO method has been demonstrated through examples of various orthotropic ratios.

It is noted that by modifying the material interpolation function, the method is applicable to the design of orthotropic composite materials.

Acknowledgements

The work conducted in this paper is supported by Australian Research Council under its Discovery Projects funding scheme (No. DP1094403), and the National Natural Science Foundation of China (No. 10872036).

References

[1] Z. Gürdal, R.T. Haftka, P. Hajela, Design and Optimization of Laminated Composite Materials, Wiley Interscience, 1999.
[2] I.D. Cave, L. Hutt, Wood Sci. Tech. 2 (1968) 268–278.
[3] L.J. Gibson, M.F. Ashby, B.A. Harley, Cellular Materials: in Nature and Medicine, Cambridge University Press, 2010.
[4] E.I. Saavedra Flores, M.S. Murugan, M.I. Friswell, E.A. de Souza Neto, Procedia Eng. 10 (2011) 3616–3621.
[5] R. Lipton, Proc. R. Soc. London A 443 (1994) 399–410.
[6] P. Pedersen, Struct. Optim. 2 (1990) 55–63.
[7] P. Pedersen, Struct. Optim. 26 (2004) 37–49.
[8] M.P. Bendsøe, N. Kikuchi, Comput. Methods Appl. Mech. Eng. 71 (1988) 197–224.
[9] M.P. Bendsøe, O. Sigmund, Topology Optimization – Theory, second ed., Methods and Applications, Springer, 2003.
[10] O. Sigmund, Mech. Mater. 20 (1994) 351–368.
[11] O. Sigmund, J. Mech. Phys. Solids. 48 (2000) 397–528.
[12] O. Sigmund, Int J. Solids. Struct. 31 (1994) 2313–2329.
[13] S. Sturm, S. Zhou, Y.W. Mai, Q. Li, J. Biomech. 43 (2010) 1738–1744.
[14] O.M. Querin, Y.M. Xie, G.P. Steven, Eng. Comput. 15 (1998) 1031–1048.
[15] X.Y. Yang, Y.M. Xie, G.P. Steven, O.M. Querin, AIAA J. 37 (1999) 1483–1488.
[16] V. Young, O.M. Querin, G.P. Steven, Y.M. Xie, Struct. Optim. 18 (1999) 183–192.
[17] X. Huang, Y.M. Xie, Evolutionary Topology Optimization of Continuum Structures: Methods and Applications, John Wiley & Sons, 2010.
[18] X. Huang, A. Radman, Y.M. Xie, Comp. Mater. Sci. 50 (2011) 861–870.
[19] X.Y. Yang, X. Huang, Y.M. Xie, Q. Li, J.H. Rong, Int. J. Optim. Civil Eng. 3 (2011) 397–417.
[20] B. Hassani, E. Hinton, Comput. Struct. 69 (1998) 707–717.
[21] S. Zhou, Q. Li, J. Phys. D: Appl. Phys. 40 (2007) 6083–6093.
[22] G.I.N. Rozvany, M. Zhou, T. Birker, Struct. Optim. 4 (1992) 250–254.